Engineering Applications of Computational Fluid Mechanics Vol. 3, No. 2, pp. 258–270 (2009)

# NUMERICAL INVESTIGATION OF FLOW IN THE VICINITY OF A SWIMMING JELLYFISH

Matevž Dular*, Tom Bajcar and Brane Širok

*University of Ljubljana, Aškerčeva 6, 1000 Ljubljana, Slovenia*
** E-Mail: matevz.dular@fs.uni-lj.si* (*Corresponding Author*)

**ABSTRACT:** The paper deals with the simulation of unsteady flow around jellyfish *Aurelia* sp. with consideration of the cyclic behaviour of the jellyfish bell. The bell cyclic movement was extracted from the video recordings of a swimming jellyfish while its displacement was simultaneously calculated from the numerically predicted forces of the bell on the fluid. Numerical simulation enabled us to predict the time evolution of the velocity field in the vicinity of the jellyfish and the formation of vortex rings that were observed during experiments. Comparison with experimental investigations revealed a good correlation in the flow pattern between forces and swimming velocity. Because of a relatively simple problem set-up the study also indicates a good possibility for further numerical studies of locomotion of organisms where experiments are hard or impossible to perform. Additionally a hypothesis that the organism uses a slightly asymmetric swimming technique to preserve a symmetric flow field was formulated.

**Keywords:** Computational Fluid Dynamics, jellyfish, propulsion

## 1. INTRODUCTION

Morphological characteristics affect swimming and foraging behaviour and *Aurelia* sp. has been classified as an oblate medusa having a rowing mode of propulsion and lower swimming performance, which create high fluid disturbance. Understanding the motion of Aurelia and the dynamics of a vortex ring is important for species ecology (Dabiri, Colin and Costello, 2006).

The importance of medusae propulsion for their displacement (swimming) and predation has been recognized since the early 1970s (Gladfelter, 1972 & 1973), and our understanding of the swimming and feeding of medusae has increased substantially in the last few decades—Mills (1981), Costello and Colin (1994) and Ford, Costello and Heilderberg (1997). Also different models have been developed to describe medusae jet propulsion (Daniel, 1983), swimming (Matanoski and Hood, 2006) and the generated flow patterns (Dabiri et al., 2005; Shaden, Dabiri and Marsden, 2006; Dabiri, Colin and Costello, 2006).

One of the obvious problems when experimenting with living organisms is their cooperation. It is extremely difficult to obtain quality experimental data, especially if the measurements involve techniques like acquisition of time dependant velocity field, which is essential for studying jellyfish locomotion—Dabiri, Colin and Costello (2007). The problem can be avoided by using computational fluid dynamics to simulate the situation in question. CFD is widely utilized in almost all technical fields but has not been used to simulate the flow around a swimming medusa yet. This is mainly because the description of the jellyfish bell motion in CFD was not possible until dynamic mesh and immersed boundary methods were developed to tackle the problem.

The dynamic mesh tool is used to model flows where the shape of the domain is changing with time due to motion on the domain boundaries. The update of the volume mesh is handled automatically at each time step based on the new positions of the boundaries. To use the dynamic mesh model, one needs to provide a starting mesh and the description of the motion. The numerical simulation of dynamically updated meshes arises in many engineering applications like moving boundary problems, bio-fluid mechanics problems and fluid-structure interaction problems (Zeng and Ethier, 2005; Cavagna, Quaranta and Mantegazza, 2007; Tai, Liew and Zhao, 2007).

The present paper deals with an unsteady simulation of the flow around jellyfish *Aurelia* sp. with consideration of the cyclic behaviour of the jellyfish bell. The forces generated by bell contraction were predicted and displacements of the jellyfish were calculated. Evolution of the velocity field around the jellyfish was predicted. Finally the spreading of the "numerical dye" injected from a determined point in space and time and the development of vortex rings were observed. A comparison of numerical predictions to the experimental results of the present study

*Received: 2 Sep. 2008; Revised: 10 Dec. 2008; Accepted: 17 Dec. 2008*

and past studies by other authors (Dabiri, 2005; Shaden, Dabiri and Marsden, 2006; Dabiri, Colin and Costello, 2006; Franco et al., 2007) gave a close approximation.

This paper describes the first study where the capabilities of CFD were evaluated. It is shown that simulations can bring a new look into the flow dynamics and can help significantly to interpret experimental results. The successfully finished and relatively unproblematic study shows good possibilities for further numerical studies of locomotion of organisms where experiments are hard or impossible to perform.

Additionally a hypothesis was formulated that the jellyfish uses a slightly asymmetric stroke to keep the downstream wake symmetric and optimal from the swimming efficiency point of view.

## 2. EXPERIMENT

The main goal of the present work was to perform a successful simulation of jellyfish swimming. In order to do that, we first had to study the dynamics of the jellyfish bell and the general characteristics of the surrounding flow.

*Aurelia* sp. were observed in June 2006 while they were swimming in a large aquarium (Cretaquarium, Thalassocosmos, Greece).

Standard video recordings were made to define movements. Image acquisition frequency was 25 Hz, which gives a time difference of 0.04 s between two successive images.

The cycles differed in duration and varied from about 3.5 s to 5.5 s. For our test case a 4.16 s long cycle that contained the whole period (jellyfish bell relaxation and contraction phases) was used. The sequence is shown in Fig. 1 (the time difference between the images is 0.48 s).

One can see that the jellyfish first starts to relax—its bell spreads from the totally contracted position to totally relaxed position in about 2.6 s. After that a faster contraction period follows. The bell attains its most contracted shape in a little less than 1.5 s. While very small and usually negligible forces between the bell and the fluid exist during the relaxation phase, much greater forces that eventually lead to movement are present during the contraction phase.

Maximal diameter of the jellyfish is reached in the relaxed position, just before the contraction phase begins. At that point a bell diameter of 150 mm was estimated.

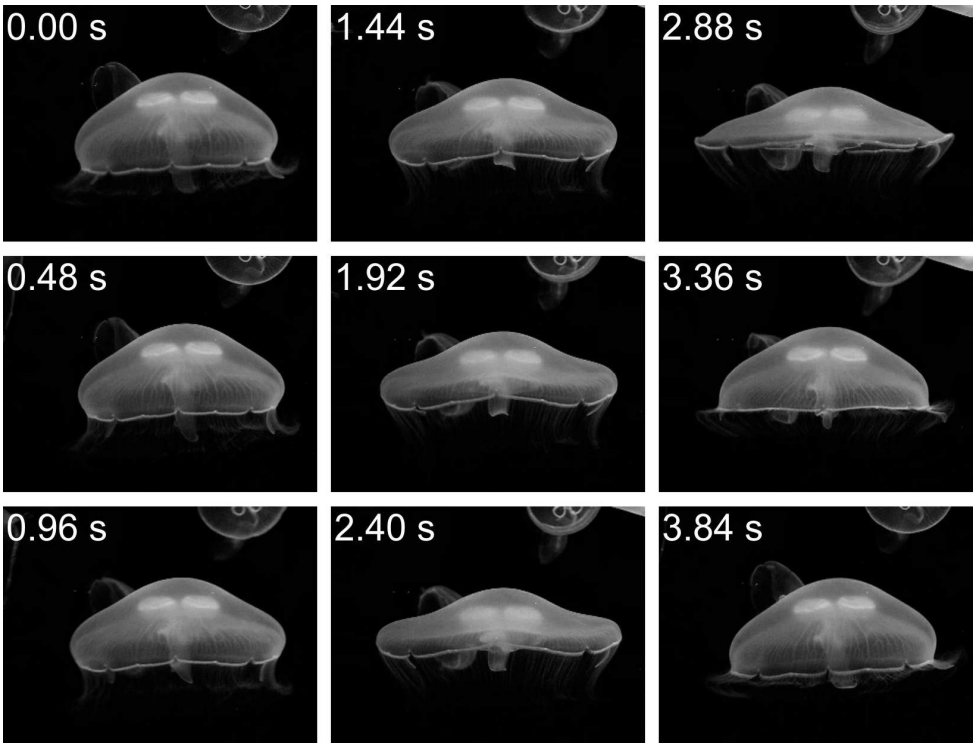


Fig. 1 A sequence of images showing the relaxation and contraction of the jellyfish bell.

### 2.1 Determination of bell shape

The bell pulsation cycle of medusa was determined by computer-aided visualization. The whole process was performed using the Matlab program package. Since the purpose of this part of the work was to determine the movement of the bell that was later used as an input for the numerical simulation, an assumption of symmetrical shape of the bell was made. Only the right side of the bell was studied further on.

First a transformation of each video image in the sequence into a binary image, with the outer contour of the *Aurelia* sp. bell clearly visible, was made.

The Sobel method (Sobel, 1978) for edge detection was used to determine the outer contour of the medusa bell.

A translation of the contour was then made so that the bell top always remained in the origin of the coordinate system (x=0, y=0). This enabled a simpler formulation of equations of bell movement. Moreover it is much easier to deform a mesh and preserve high mesh quality later on in CFD when one point remains fixed at all time.

The image resolution was 640×480 pixels so one half of the bell occupied about 320 pixels. The current position of the contour was determined for every 15 pixels from the centre of the image. This led to 23 equidistant points (given by x and y coordinates) that lay on the contours of the bell. Finally it was decided that a polynomial fit of the 6th order is the optimal way to determine the equation of the contour. Polynomial fits are easy to use, and the 6th polynomial order gives a sufficient agreement and on the other hand does not complicate the equation with very small factors:

$$y_{out} = a_6x^6 + a_5x^5 + a_4x^4 + a_3x^3 + a_2x^2 + a_1x + a_0 \tag{1}$$

In order to describe the contour by a parametric function $y = f(x)$ the coordinate system had to be rotated for each part of the bell contour (Fig. 2).

This way we mathematically described the shape of the outer contours for each bell shape in the sequence.

It was recently shown by Bajcar et al. (2009) that the inner bell contour is dependent on the shape of the outer contour. A function:

$$y_{in} = y_{out} - k \cdot (x - x_{\max}) \tag{2}$$

was used to describe it. The k gives the gradient at which the thickness of the bell decreases from the bell centre to the bell perimeter. It was also found by Bajcar et al. (2009) that the bell thickness decreases approximately linearly. Also the diameter of the bell changes, therefore $x_{max}$ varies from one image to another depending on the current diameter of the jellyfish.

Finally a transformation of the polynomials of the right contours to the symmetrical left contours was made. A sample image showing the left side of the jellyfish bell and superimposed polynomial functions that mathematically determine the bell shape are presented in Fig. 2.

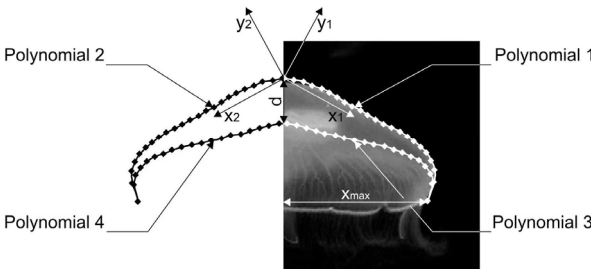


Fig. 2 Jellyfish image in a coordinate system with superimposed polynomial functions.

One cycle of bell relaxation and contraction was eventually split into 52 steps of 0.08 s each. For every single step 4 polynomials were used to determine the bell shape—one for every part of the bell (outer left—polynomial 1, outer right—polynomial 2, inner left—polynomial 3 and inner right—polynomial 4):

$$\begin{aligned}
&\text{Polynomial 1: } y_1 = a_6x_1^6 + a_5x_1^5 + a_4x_1^4 + a_3x_1^3 + a_2x_1^2 + a_1x_1 + a_0\\
&\text{Polynomial 2: } y_2 = a_6x_2^6 - a_5x_2^5 + a_4x_2^4 - a_3x_2^3 + a_2x_2^2 - a_1x_2 + a_0\\
&\text{Polynomial 3: } y_1 = a_6x_1^6 + a_5x_1^5 + a_4x_1^4 + a_3x_1^3 + a_2x_1^2 + (a_1 + k)x_1 + (a_0 - d)\\
&\text{Polynomial 4: } y_2 = a_6x_2^6 + a_5x_2^5 + a_4x_2^4 + a_3x_2^3 + a_2x_2^2 - (a_1 + k)x_2 + (a_0 - d)
\end{aligned} \tag{3–6}$$

where $a_6$, $a_5$, $a_4$, $a_3$, $a_2$, $a_1$, $a_0$ and k are time dependent variables and d, the maximal thickness of the bell, is constant. One can see that polynomials 3 and 4 describe the inner contour of the bell. Because the thickness of the bell decreases linearly with k, the rate at which the bell thickness decreases towards the

perimeter of the bell is present in the linear term of the polynomial. d gives the maximal thickness of the bell and remains constant for all images—it is therefore included at the constant term of the polynomial.

### 2.2 Characteristics of the flow around the jellyfish

For numerical simulation, flow characteristics around the body of the jellyfish have to be considered.

To determine whether the flow is laminar or turbulent, which consequently leads to the choice of the model that we use for the simulation, the Reynolds number has to be determined:

$$\mathrm{Re} = \frac{\rho v \cdot 2 \cdot x_{\max}}{\mu} \tag{7}$$

While the characteristic size $x_{max}$, the jellyfish bell radius, and the fluid viscosity are known, the velocity have to be estimated from the images—the position of the camera was not constant so the velocity of swimming could not be determined directly since there was no reference point in the image that did not change its position.

In our case the jellyfish swam at a relatively low pace so an assumption was made that the inertia is small and that consequently the bell progresses for the same distance as its height increases during the contraction phase. In other words, the jellyfish remains at a standstill during the relaxation phase and the margin of the bell holds its position while the bell apex progresses during the contraction phase (Fig. 3a). Since the time difference Δt and the displacement Δy were known, the velocity ($\Delta y/\Delta t$) and consequently Re number could be estimated. Figure 3b shows the approximate time evolution of the Reynolds number during one cycle of bell relaxation and bell contraction.

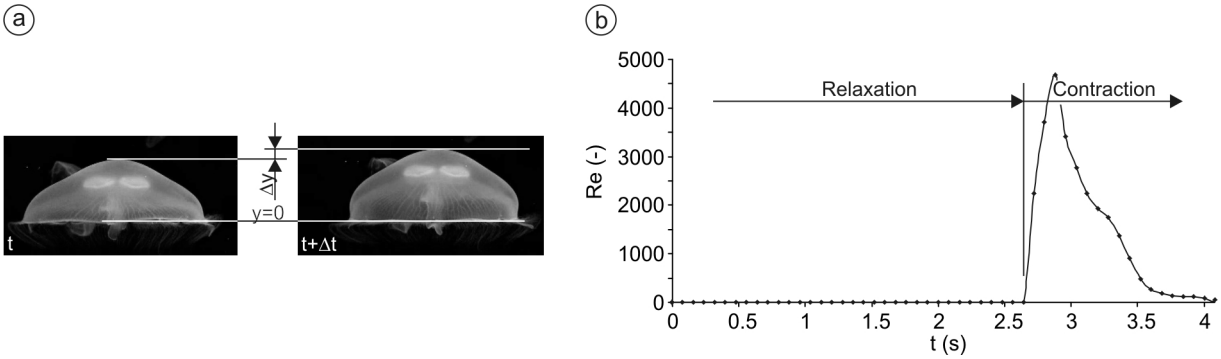


Fig. 3 (a) Method of estimating the velocity of swimming and (b) the Re number evolution.

It can be seen that the estimation shows that the Re number does not exceed a value of 5000. It would be therefore incorrect to assign a fully developed turbulent flow regime. The Re number also varies significantly in time, from fully laminar to partially turbulent flow. Moreover the assumption that the bottom of the jellyfish bell holds its position during the contraction phase is not entirely correct but we are on the safe side—the bottom of the jellyfish must also move downwards during relaxation so that the actual velocity change is smaller than what is estimated. In comparison Ichikawa, Yazaki and Mochizuki, (2006) experimentally studied the flow around *Aurelia* sp in detail and estimated that the flow does not develop turbulent characteristics. They reported that the average Reynolds number reaches up to a value of 680.

It was concluded that on the basis of the above stated reasons, a simulation with laminar flow assumption is to be performed.

## 3. NUMERICAL SIMULATION

A program package Fluent 6.2.16 was used to calculate the flow around the jellyfish. It solves a set of time dependent Navier-Stokes equations in a conservative form. The numerical model uses an implicit finite volume scheme, based on the SIMPLE algorithm (Patankar, 1980). A 1st order implicit temporal discretization and 2nd order upwind differentiating scheme were used. In the present study the numerical problem was treated as a 2-dimensional problem.

### 3.1 Basic equations of fluid dynamics in moving grids

By adopting the laminar flow characteristics no averaging of the basic Navier-Stokes equations needs to be performed. Moreover the fluid (sea water) can be considered incompressible $\rho=\rho_0$, which further on simplifies the set of equations. Consideration of deforming a domain, however, requires a slight modification of the equations where the difference between the flow velocity and the grid velocity $\vec{u}-\vec{u}_g$ is used for the convective terms.

If an incompressible fluid is considered, the mass and the momentum conservation equations that form a closed system of equations read:

$$\nabla\cdot\left(\vec{u}-\vec{u}_g\right)=0 \tag{8}$$

and

$$\frac{\partial\vec{u}}{\partial t}+\nabla\cdot\left[\left(\vec{u}-\vec{u}_g\right)\vec{u}\right]=-\frac{1}{\rho_0}\nabla p+v_0\nabla\cdot\left(\nabla\vec{u}\right) \tag{9}$$

### 3.2 Dynamic mesh update methods

First the domain with an initial geometry was manually meshed. The initial computational domain extended 1 by 1 m at the centre of which was the contour of the jellyfish in a totally contracted position (Fig. 4).

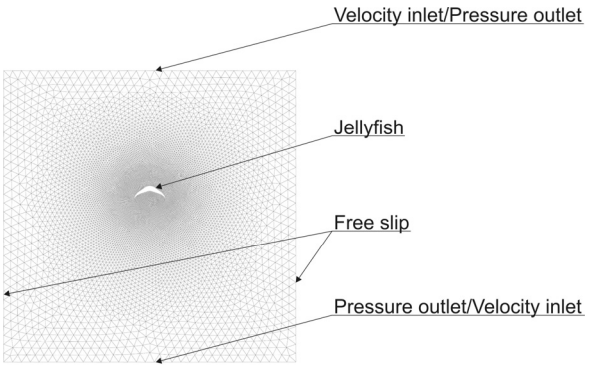


Fig. 4 Initial computational domain with mesh and boundary conditions.

The mesh consisted of about 17000 nodes that defined the triangular elements. The size of elements had to be adjusted according to minimal discretization error on one hand and by so doing to avoid problems at mesh updating on the other.

To check the influence of spatial discretization, a study of the discretization error on the basis of the Richardson extrapolation (Ferziger and Perić, 1999) was made. An error of 0.9 % was estimated.

The choice of the length of the time step can be influential to the result and the stability of simulation. From previous investigations dealing with complex time dependent flow structures (Dular et al., 2005) we concluded that at least 40 to 50 time steps per cycle must be used to avoid adverse impact on results, to work with reasonable computational time and to retain stable simulation. Eventually, 52 time steps of 0.08 s each were used to describe one cycle—the same number as the number of images that captured one cycle of jellyfish movement in the experiment. As time progresses the jellyfish periodically changes its shape. To follow this movement the mesh must constantly (at each time step) be updated. In our case smoothing and local remeshing techniques were applied (Batina, 1990). To test the quality and the robustness of the mesh update method, maximal cell equiangle skew value was determined for each time step during the simulation. It was determined that the mesh first deteriorates from the initially low value of maximal cell equiangle skew but then, despite the large deformation of the domain, preserves a still plausible value of cell equiangle skew <0.7.

### 3.3 Boundary conditions

Translation of the jellyfish was treated from a relative point of view. At the end of every time step the forces of the jellyfish on the fluid or vice versa were calculated. When the forces were known, the acceleration and finally flow velocity at the inlet into the computational domain for the next time step could be calculated using:

$$v(t)=v(t-\Delta t)+\frac{\sum_i F_i}{m}\cdot\Delta t \tag{10}$$

where the force component along the specified vector $\vec{a}$ on a wall zone $i$ is computed by summing the dot product of the pressure and viscous forces on each face with the specified vector. The mass of the jellyfish was estimated according to its volume, which is constant in time, and the fact that it consists of almost 100% water. This method is not entirely correct since forces from a previous time step are used to determine the velocity in the next time step, but since the time steps were sufficiently short, the error made can be considered negligible. Also a possibility of reverse flow was considered in the case of which the inlet and the outlet boundary conditions swapped places.

The side walls of the domain had a free slip boundary condition applied. The values

$\rho = 1025\ \mathrm{kgm^{-3}}$ and $\mu = 10^{-3}$ Pa s for sea water density and dynamical viscosity were used for the simulation.

### 3.4 Calculation procedure

Fig. 5 shows the steps taken during the calculation.

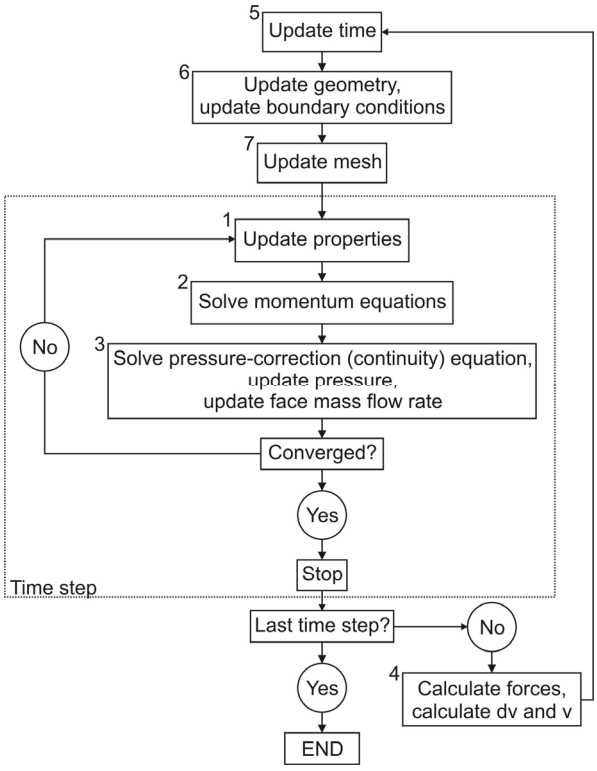


Fig. 5 Solution algorithm.

The solution algorithm solves the governing equations sequentially. Because the governing equations are non-linear (and coupled), several iterations of the solution loop must be performed before a converged solution is obtained. The solution procedure follows the steps illustrated in Fig. 6 and is outlined below:

1. Fluid properties are updated, based on the current solution. If the calculation has just begun, the fluid properties are updated based on the initialized solution.
2. Each of the momentum equations is solved in turn using current values for pressure and face mass fluxes, in order to update the velocity field.
3. Since the velocities obtained in the second step may not satisfy the continuity equation locally, an equation for the pressure correction is derived from the continuity equation and the linearized momentum equations. This pressure correction equation is then solved to obtain the necessary corrections to the pressure and velocity fields and the face mass fluxes such that continuity is satisfied.

A check for convergence of the equation set is made. If the convergence criteria are not met, steps 1 to 3 are continued until convergence is obtained.

4. Resultant of the forces of fluid on the body or vice versa is calculated. Using Eq. (10) acceleration and consequently the body velocity are calculated.
5. The time is updated to $t = t + \Delta t$.
6. A new geometry of the body is calculated according to Eqs. (3) to (6) and the boundary conditions are updated—new inlet velocity is set according to the result of Eq. (10).
7. Mesh is updated.
8. An iteration procedure for the new time step begins.

These steps are continued until the last time step. The criterion for a converged time step solution was determined by observation of static pressure at the inlet of the computational domain. Within one time step the value of static pressure always converged when the sum of the residuals decreased by 3 orders of magnitude. We additionally compared solutions at different convergence criteria ($5\times10^{-4}$ and $5\times10^{-5}$) but found no significant difference in results. Finally a convergence criterion of $10^{-4}$ was used to minimise iteration error but not to additionally extend computational time. The iteration error of 0.05% was estimated according to Ferziger and Perić (1999). Approximately 40 iterations per time step were needed to obtain a converged time step solution.

## 4. RESULTS

Results of simulation were compared to the results of previous experiments done by other authors. The results of numerical simulation and experimental results cannot be compared quantitatively, since the “experimental” and “numerical” jellyfish differed in size and cycle length. The jellyfish species was the same in all cases—*Aurelia* sp. Nevertheless a good approximation was found in all cases, which points to the significant potential of using

numerical simulations for easier and more in-depth interpretation of organism locomotorics.

### 4.1 Propulsion forces

One of the obvious parameters that are close to impossible to determine experimentally is the force on the fluid applied by the organism. Different methods were described by Usherwood et al. (2007), Dabiri (2005) and Peng et al. (2007) but they are either indirect or not applicable to jellyfish.

In computational fluid dynamics this problem can be easily avoided. The pressure field is known at every time the force can be easily deducted. Figure 6 shows the time evolution of the forces on the fluid.

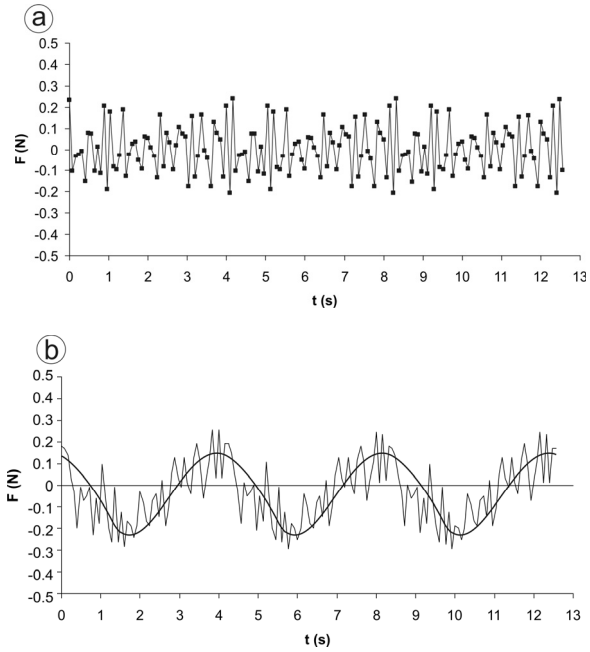


Fig. 6 Time evolution of the force during several cycles.

The jellyfish contracted and relaxed symmetrically so the sum of forces applied in the perpendicular direction to the flow is equal to zero.

It can be seen that the force in the direction parallel to the jellyfish motion oscillates quite a lot, but generally the evolution follows a pattern plotted in the bottom diagram (Fig. 6b), which was generated by averaging 10 sequential time steps in a package (moving average technique). Although it is hard to distinguish any periodic nature in Fig. 6, we can claim that in general the force is negative during the relaxation phase, which forces the jellyfish downwards and increases rapidly during the contraction phase, which results in forward movement.

### 4.2 Jellyfish displacement

We already mentioned that the actual jellyfish displacement could not be measured during the present experiment since the camera moved and no stationary reference point could be determined. For evaluation of the numerical simulation the actual jellyfish displacement was determined on the basis of a movie made by Shadden, Dabiri and Marsden (2006). During that experiment the camera remained at a determined position while the jellyfish swam by it, so the determination of the displacement was trivial. Bell apex was chosen as a reference point of the jellyfish, so its distance from the reference point was measured for each image. The uncertainty of this method is relatively high since the resolution of the images was low. The measured displacement of the jellyfish as a function of time can be seen in Fig. 7.

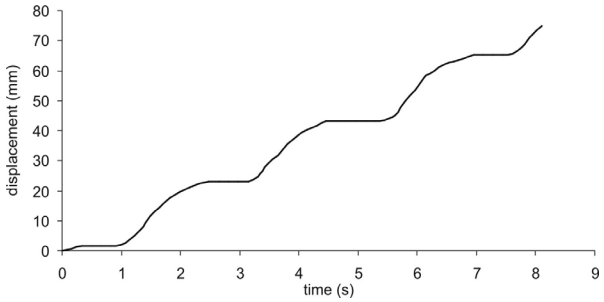


Fig. 7 Measured jellyfish displacement (on the basis of a movie by Shadden, Dabiri and Marsden (2006)).

It was expected that the jellyfish progresses in a distinctive stair-like manner. It remains at a standstill during the relaxation phase and moves rapidly during the contraction phase. In each bell stroke it progresses for approximately 0.021 m. The maximal velocity is achieved in the middle of the contraction phase when the bell apex reaches up to 0.027 $ms^{-1}$.

The cycle length of the jellyfish differs from 4.16 s for the case of “numerical” jellyfish to about 2.3 s for the case of “experimental” jellyfish. Similarly the diameter of the totally relaxed “numerical” jellyfish is 150 mm while the “experimental” jellyfish stretches itself only to about 110 mm. Figure 8 shows the numerically predicted jellyfish displacement.

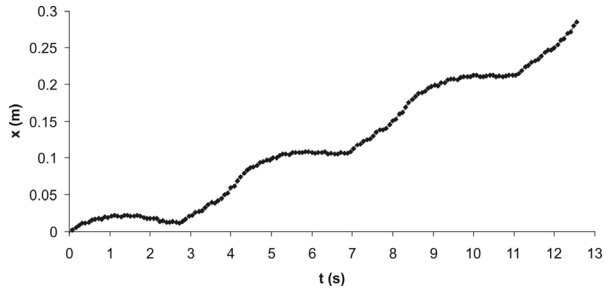


Fig. 8 Numerically predicted jellyfish displacement.

The simulation correctly predicted the manner by which the jellyfish progresses. The qualitative resemblance between the experimental and numerical results is clearly seen. It is predicted that the bell remains almost at rest during relaxation or in some cases even regressed slightly. During contraction it moves rapidly forward. On the other hand the simulation predicted that the jellyfish swims at a much faster pace. It is predicted that the bell progresses for about 0.1 m during each cycle and that it reaches a maximal velocity of 0.075 $ms^{-1}$. It is hard to compare the quantitative results since we are in fact dealing with two individual organisms—it is known that the jellyfish can move in a vast span of velocities—see for example, Dabiri, Colin and Costello (2007). It can be concluded that the simulation is in a decent agreement with a real situation in nature, but probably a much more advanced experiment will have to be performed to either confirm or reject this statement.

### 4.3 Velocity field

Data from measurements by Franco et al. (2007) were used to evaluate the numerical simulation. The velocity field in the vicinity of the jellyfish was measured using the PIV technique (Particle Image Velocimetry). The jellyfish measured approximately 100 mm in diameter in its totally relaxed position and the length of one cycle was about 5 s.

The two vector plots in Fig. 9 show the velocity field at different instants during the relaxation phase (left) and the contraction phase (right). The bottom two schemes show the approximate flow directions for the situations above.

During the relaxation phase a clear recirculation of the flow can be seen. As the jellyfish relaxes a low pressure region develops inside the bell and sucks the fluid from the outside. One can see that, since the bell is slowly stretching outwards, the flow on the outside is not directly influenced and it changes direction (towards the bell centre) only after it passes about 10 mm downstream of the bell margin. This flow pattern is practically the same for the whole period of bell relaxation.

The velocity field recorded during the contraction phase (right), seems to be similar but is in fact different. Inside the bell the flow is driven to the centre not by the pressure difference but directly due to the force applied at the contraction. On the outside of the bell the rapid contraction creates a low pressure field in the vicinity of the bell which causes the flow to follow the bell movement. Because of that the change of the flow direction occurs more upstream than during the relaxation (about 15 mm before the bell margin). A close inspection also reveals that as flow from opposing sides collides downstream of the jellyfish, two new vortices are created. These have an opposite direction to that of the vortices near the bell margin. A more thorough study of these results was conducted by Dabri et al. (2005).

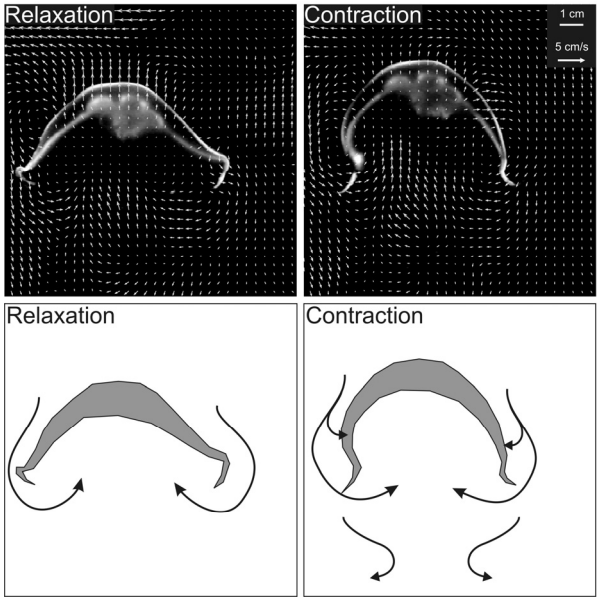


Fig. 9 Measured velocity fields at different times during swimming cycle (Franco et al., 2007).

Figure 10 shows sequence of numerically predicted velocity fields at different times in the cycle.

One cycle with the relaxation and the contraction phases are shown. As the bell relaxes, the flow is sucked from the vicinity of the jellyfish into its bell. This results in a formation of a distinctive vortex that can be well seen. The vortices continue growing until the bell relaxes. As the contraction part of the cycle begins at t=2.88 s the fluid is submitted to a force that pushes the vortices downstream. One can also see that the primary vortices (generated during bell relaxation) deteriorate in size, which is a result of pairing with counter rotating vortices that are generated during the bell contraction phase (t=3.84 s).

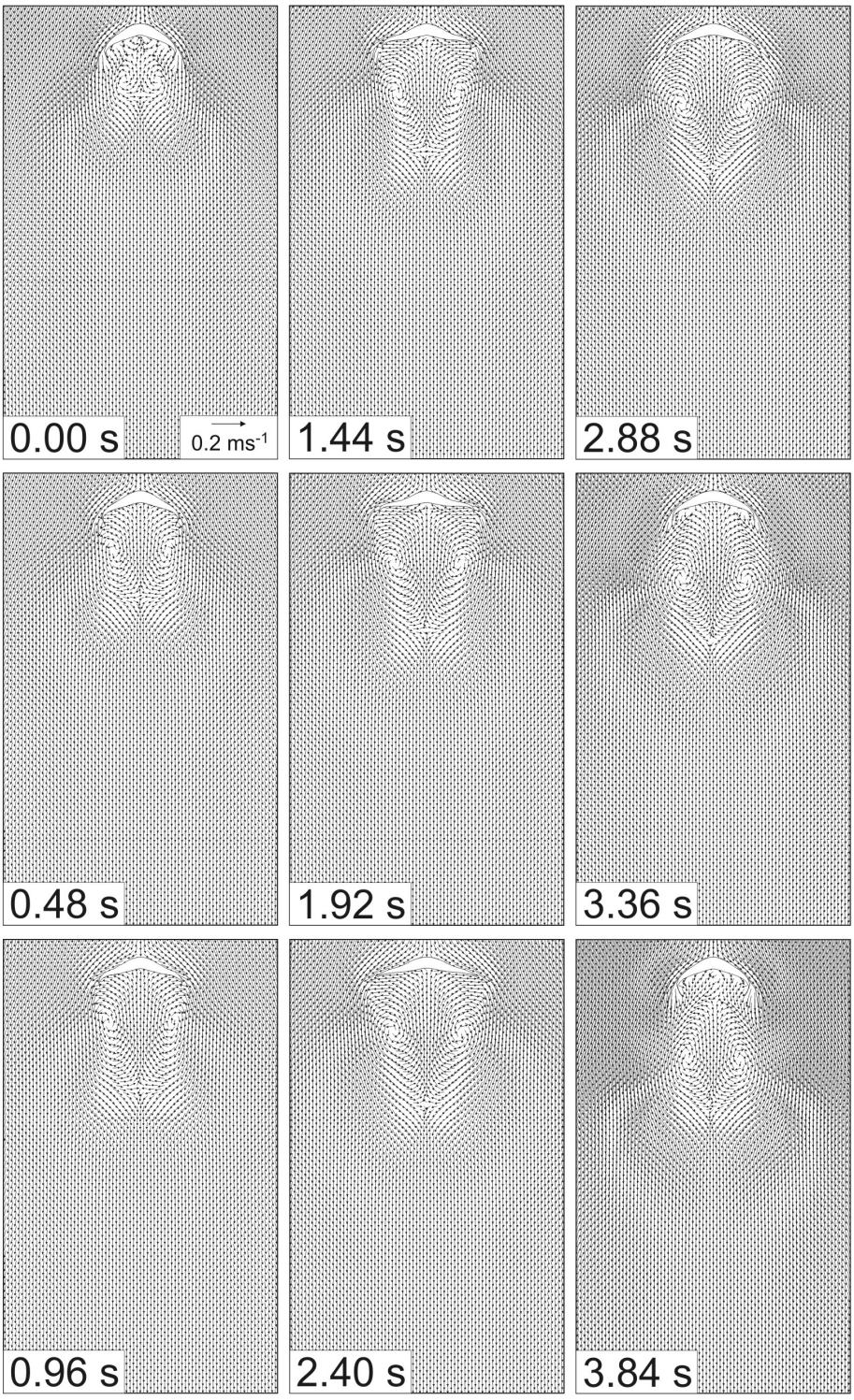


Fig. 10 Numerically predicted velocity fields at different times in swimming cycle.

As the bell contracts the fluid is squished from the inside resulting in a force that triggers movement. As the flow travels downstream it loses its momentum and starts to decelerate and form a vortex that has the opposite rotation as the one that is formed by bell relaxation.

**4.4**

**Path of numerical dye**

The experiment in Fig. 11 was conducted by Dabiri et al. (2005) where a small quantity of fluorescent dye was injected into the water surrounding the animal. The diameter of the totally relaxed jellyfish was approximately 200 mm while the cycle length lasted about 2.6 s.

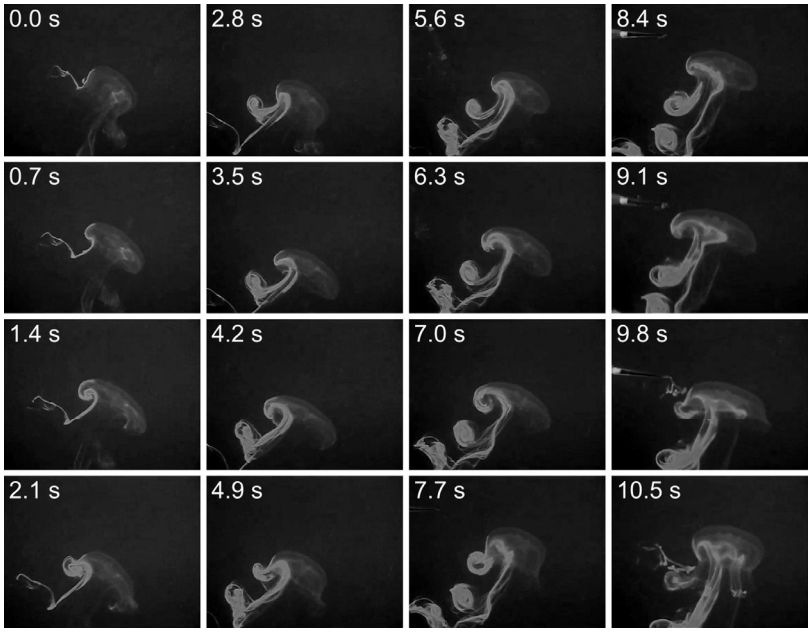


Fig. 11 Dye visualization of jellyfish vortex wake (Dabiri et al., 2005).

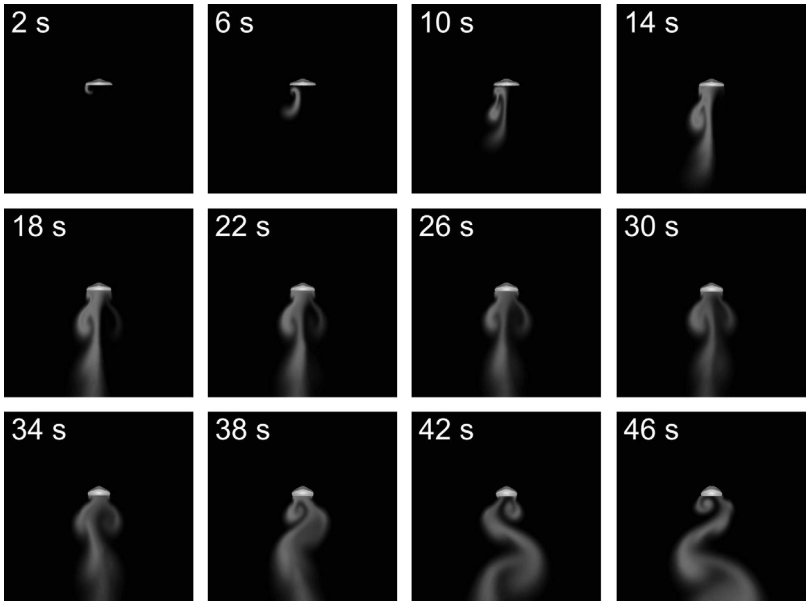


Fig. 12 Numerically predicted evolution of the vortex street.

As shown in the images the dye was injected upstream of the animal to observe the fluid motion induced by the animal as it swam forward. The formation of a vortex ring is observed as the animal contracts its body. A second vortex ring of opposite rotational sense forms as the animal relaxes to its original resting form. Subsequently, the two vortex rings pair together and develop instabilities as they propagate downstream (Dabiri et al., 2005).

The initial position time instant at which the "numerical dye" was released was selected to resemble the position and the time of injection in the experiment. Figure 12 shows the numerically predicted evolution of the vortex street behind the jellyfish. Dye was injected near the left side of the bell perimeter. As time progresses the concentration of the dye lowers and the colour scale is adjusted—this is why the dye becomes visible also on the right side of the jellyfish bell.

The jellyfish starts its cycle in a totally contracted phase. At this instant a small amount of "numerical dye" was placed above the bell on the left side. It can be seen that as the jellyfish relaxes the dye is sucked into the bell forming a vortex. As the bell starts to contract, the dye is pushed out and flows downstream of the jellyfish. When the jet losses its momentum, it creates a secondary vortex of an opposite sense of rotation. The simulation obviously corresponds well to the real situation.

After some periods the first sign of asymmetric flow pattern becomes visible. Later, a clear oscillating vortex street forms. This was not observed in the experiment and is probably caused by a simplification where an assumption of axisymmetric bell movement was made. This aspect is more thoroughly discussed in the next section of this paper.

## 5. DISCUSSION

It is of great importance to discuss the evolution of the oscillating vortex street during the simulation. This is obviously not in agreement with experimental measurements where no such asymmetry was observed. Figure 13, for example, shows an image where vortices from 5 periods of jellyfish contraction/relaxation are seen.

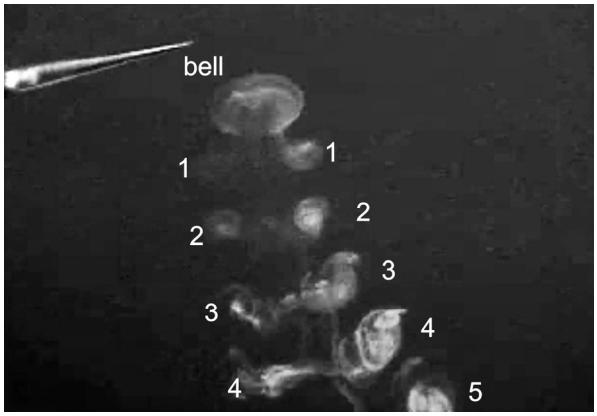


Fig. 13 Symmetric vortex street after 5 jellyfish contraction/relaxation phases (Dabiri et al., 2005).

The hypothesis is that the jellyfish probably contracts and relaxes its bell slightly asymmetrically to compensate for the development of the asymmetrical vortex street, which is from the swimming point of view less efficient and not stable.

In simulation vortices begin to shift alternatively from side to side. The differences are small and the effect cannot be seen at first, but as time passes the small differences grow and eventually a significant asymmetry develops as seen in Fig. 12. This means that it is only possible to use such simulations for predicting short term phenomena. In our case the simulation is valid for all studied parameters except the evolving wake behind the bell of the jellyfish—and even that if we consider only 4 or 5 cycles when the asymmetry is still insignificant.

## 6. CONCLUSIONS

The main purpose of this work was to evaluate the capability of numerical simulation and the first step towards in-depth numerical investigations of the flow in the vicinity of living organisms. It was shown that computational fluid dynamics coupled with not too complex methods of computer aided visualization can be a useful tool for studying complex flow around living organisms. It is particularly useful in cases where advanced experiments are expensive and hard to perform (like velocity measurements with PIV method).

It was concluded, on the basis of good qualitative correlation between the predictions and experiments, that the numerical tools are ripe for simulation of such problems.

The agreement between experiments and simulation was fair for the case of predicting jellyfish displacement evolution, velocity field and the wake when only a few periods are considered. The numerical simulation also helped to formulate a hypothesis that the jellyfish has to make small corrections in the otherwise symmetric contraction/relaxation motion to preserve the symmetric wake.

The next step is to upgrade the simulation to a 3-dimensional problem and to include the asymmetric motion of the bell to further investigate the possible presence of asymmetry. The final goal would be to include fluid structure interaction into account, but this would mean that the muscular and tissue properties of the jellyfish should be known—this is at the present time beyond the scope of simulations.

## NOMENCLATURE

| | |
|---|---|
| $a_6$, $a_5$, $a_4$, $a_3$, $a_2$, $a_1$, $a_0$ | constants in the polynomial equation (-) |
| d | thickness of bell core (m) |
| $F_i$ | force (N) |
| G, $G_x$, $G_y$ | gradients in the image (pixel value/pixel) |
| k | constant (-) |
| $k_{ij}$ | grid spring constant (N/m) |
| m | mass (kg) |
| p | pressure (Pa) |
| $q_e$ | equiangular cell angle (°) |
| $q_{max}$ | maximal cell angle (°) |
| $q_{min}$ | minimal cell angel (°) |
| Re | Reynolds number (-) |
| $S_\Phi$ | source of arbitrary variable (-) |

| | |
|---|---|
| $t$ | time (s) |
| $u$ | local velocity ($ms^{-1}$) |
| $u_g$ | grid velocity ($ms^{-1}$) |
| $v$ | integral velocity ($ms^{-1}$) |
| $x$ | coordinate (m) |
| $x_i$ | grid deformation (m) |
| $x_j$ | grid deformation (m) |
| $x_{max}$ | maximal radius of jellyfish (m) |
| $y$ | coordinate (m) |
| $y_{in}$, $y_{out}$ | coordinates of the inner and outer bell contour (m) |
| $\phi$ | arbitrary variable (-) |
| $\gamma$ | cell equiangle skew (-) |
| $\Gamma$ | diffusion coefficient (-) |
| $\mu$ | viscosity (Pa s) |
| $\mu_0$ | constant viscosity (Pa s) |
| $\rho$ | density ($kgm^{-3}$) |
| $\rho_0$ | constant density ($kgm^{-3}$) |

## REFERENCES


1. Bajcar T, Malačič V, Malej A, Širok B (2009). Kinematic properties of the jellyfish Aurelia sp. *Hydrobiologia* 616(1):279–289.
2. Batina JT (1990). Unsteady Euler airfoil solutions using unstructured dynamic meshes. *AIAA Journal* 28(8):1381–1388.
3. Costello JH, SP Colin (1994). Morphology, fluid motion and predation by the scyphomedusa. *Aurelia aurita*. *Mar. Biol.* 121:327–334.
4. Cavagna L, Quaranta G, Mantegazza P (2007). Application of Navier-Stokes simulations for aeroelastic stability assessment in transonic regime. *Computers and Structures* 85:818–832.
5. Dabiri JO (2005). On the estimation of swimming and flying forces from wake measurements. *J. Exp. Biol.* 208:3519–3532.
6. Dabiri JO, Colin SP, Costello JH (2006). Fast-swimming hydromedusae exploit velar kinematics to form an optimal vortex wake. *Journal of Experimental Biology* 209(11):2025–2033.
7. Dabiri JO, Colin SP, Costello JH (2007). Morphological diversity of medusan lineages constrained by animal-fluid interactions. *Journal of Experimental Biology* 210(11):1868–1873.
8. Dabiri JO, Colin SP, Costello JH, Gharib M (2005). Flow patterns generated by oblate medusan jellyfish: field measurements and laboratory analyses. *Journal of Experimental Biology* 208(7):1257–1265.
9. Daniel TL (1983). Mechanics and energetics of medusan jet propulsion. *Can. J. Zool.* 61(6):1406–1420.
10. Dular M, Bachert R, Stoffel B, Širok B (2005). Experimental evaluation of numerical simulation of cavitating flow around hydrofoil. *European Journal of Mechanics—B/Fluids* 24:522–538.
11. Ferziger JH, Perić M (1999). *Computational Methods for Fluid Dynamics*. 2nd ed., Springer Verlag.
12. Ford MD, Costello JH, Heilderberg KB (1997). Swimming and feeding by the scyphomedusa Chrysaora quinquecirrha. *Mar. Biol.* 129:355–362.
13. Franco E, Pekarek DN, Peng J, Dabiri JO (2007). Geometry of unsteady fluid transport during fluid-structure interactions. *Journal of Fluid Mechanics* 589:125–145.
14. Gladfelter WB (1972). Structure and function of the locomotory system of the Scyphomedusa Cyanea capilata. *Mar. Biol.* 14:150–160.
15. Gladfelter WB (1973). A comparative analysis of the locomotory systems of medusoid Cnidaria. *Helgolnder wiss. Meeresunters.* 25:228–272.
16. Ichikawa S, Yazaki Y, Mochizuki O (2006). Flow induced by jellyfish. *Physics of Fluids* 18, 091104.
17. Matanoski JC, Hood RR (2006). An individual-based numerical model of medusa swimming behaviour. *Mar. Biol.* 149:595–608.
18. Mills CB (1981). Diversity of swimming behaviours in hydromedusae as related to feeding and utilization of space. *Mar. Biol.* 64:185–189.
19. Patankar SV (1980). *Numerical Heat Transfer and Fluid Flow*. Hemisphere, New York.
20. Peng J, Dabiri JO, Madden PG, Lauder GV (2007). Non-invasive measurement of instantaneous forces during aquatic locomotion: A case study of the bluegill sunfish pectoral fin. *Journal of Experimental Biology* 210 (4):685–698.
21. Shadden SC, Dabiri JO, Marsden JE (2006). Lagrangian analysis of fluid transport in empirical vortex ring flows. *Physics of Fluids* 18, 047105.
22. Sobel I (1978). Neighborhood coding of binary images for fast contour following and general array binary processing. *Comput. Graphics Image Proc*. 8:127–135.

23. Tai CH, Liew KM, Zhao Y (2007). Numerical simulation of 3D fluid-structure interaction flow using an immersed object method with overlapping grids. *Computers and Structures* 85:749–762.
24. Usherwood JR, Hedrick TL, McGowan CP, Biewener AA (2007). Dynamic pressure maps for wings and tails of pigeons in slow, flapping flight and their energetic implications. *The Journal of Experimental Biology* 208:355–369.
25. Zeng D, Ethier CR (2005). A semi-torsional spring analogy model for updating unstructured meshes in 3d moving domains. *Finite Elem. Anal. Des*. 41(11–12):1118–1139.